Elastic dynamics and tidal migration of grounding lines modify subglacial lubrication and melting

R. Sayag[1] and M. Grae Worster[1]

Received 8 September 2013; revised 24 October 2013; accepted 24 October 2013.

[1] We combine the dynamics of ice, bed, and ocean in a new elastic model for the tidal-timescale migration of grounding lines on deformable foundations. Previous interpretations of tidal flexure using models of elastic ice shelves with fixed grounding lines were found to be inconsistent, suggesting an elasticity of ice that varies spatially and temporally and that is significantly smaller than measured experimentally. We argue here that with our model, a consistent, purely elastic interpretation can be made. Combining this new approach with remote-sensing measurements, we show that the grounding line migrates several kilometers during a tidal cycle, that we can infer the effective elastic properties of the bed, and that the elastic pressure of the ice leads to a hydrological barrier near the grounding line that controls subglacial hydrology. Our findings imply that subglacial lubrication and melting induced by the ocean thermal forcing can increase substantially during high tide.
Citation: Sayag, R., and M. Grae Worster (2013), Elastic dynamics and tidal migration of grounding lines modify subglacial lubrication and melting, *Geophys. Res. Lett.*, *40*, doi:10.1002/2013GL057942.

1. Introduction

[2] Grounding zones of marine ice sheets are interfaces between grounded and floating ice. The response of such regions to tidal forcing correlates with ice-flow acceleration [*Bindschadler et al.*, 2003; *Anandakrishnan et al.*, 2003; *Gudmundsson*, 2006] and is an indicator of the grounding line (GL) position [*Rignot et al.*, 2011], knowledge of which is required to determine the ice flux to the ocean and the consequent contribution to sea level rise.

[3] Previous interpretations of tidal flexure using elastic models included only the floating shelves, clamped at a fixed GL over a stiff bed (*stiff-fixed* models, Figures 1a and 1b) [*Holdsworth*, 1977]. Such models predicted ice elasticity that varies significantly between different glaciers [*Vaughan*, 1995; *Rignot*, 1996; *Sykes et al.*, 2009] that varies with tidal phases in the same glacier [*Schmeltz et al.*, 2002] and is significantly smaller than measured experimentally [*Gammon et al.*, 1983]. These discrepancies have led to the inclusion of viscous deformation in the modeling of tidal flexure [*Reeh et al.*, 2003; *Gudmundsson*, 2011; *Walker et al.*, 2013].

[4] Alternatively, such discrepancies may have resulted from misinterpreted data due to the absence of grounded-ice dynamics in past elastic models. This argument is supported by observational evidence of tidal migration of GLs [*Brunt et al.*, 2011] and of substantial bending that extends several kilometers upstream from the GL [*Jacobel et al.*, 1994], in addition to correlation with periodic accelerations of grounded ice. These observations together with evidence of thick layers of deformable sediments near GLs [*Anandakrishnan et al.*, 2007] indicate that the coupling of the shelf to the grounded sheet can be important to the interpretation of tidal flexure and subglacial processes near GLs.

2. Grounding Line Dynamics Under Tidal Forcing

[5] Scaling analysis of the forces involved in viscous bending of an ice sheet under tidal forcing implies that the flexure of ice on tidal timescales is dominantly elastic (see supporting information). We therefore consider the instantaneous deformation under tidal forcing of an elastic sheet of density ρ_i supported by an ocean of density $\rho_w > \rho_i$ and an elastically deformable bed with effective stiffness k_0, and a free GL at x_g (the *soft-free* model, Figures 1a and 1b). The sheet is assumed to have uniform thickness H and bending stiffness $D = EH^3/12(1-\nu^2)$, where E and ν are Young's modulus and Poisson ratio, respectively. Under small deflections, the vertical force balance in the floating and grounded parts is given by the Euler-Bernoulli equation

$$D\nabla^4 y = \begin{cases} -\rho_i g H + k_0\,(H/2 - y + y_b) & x \le x_g, \\ -\rho_i g H + \rho_w g\,(H/2 - y) + \rho_w g T & x_g \le x, \end{cases} \tag{1}$$

where y is the midsurface deflection of the sheet with respect to sea level along the horizontal coordinate x, $y_b(x) = -Sx$ is the undeformed shape of the bed with slope S, and T is the sea level relative to its mean. Solutions of (1) have undulations that are damped exponentially away from the GL with relaxation lengths proportional to $\ell \equiv (D/\rho_w g)^{1/4}$ in the floating shelf and to ℓ/K in the grounded sheet, where $K = (k_0/\rho_w g)^{1/4}$ (supporting information). In the stiff bed limit ($k_0 \to \infty$), the solution has been found to be in good agreement with laboratory experiments [*Sayag and Worster*, 2011].

[6] The capacity of the bed to deform results in the GL position shifting by a distance of about $\rho_i H/(\rho_w S K^2)$ relative to the GL position on a stiff bed, which can be several kilometers (supporting information). The stiffness k_0, which we use as a fitting parameter, represents an effective spring

Additional supporting information may be found in the online version of this article.

[1]Institute of Theoretical Geophysics, Department of Applied Mathematics and Theoretical Physics, University of Cambridge, Cambridge, UK.

Corresponding author: R. Sayag, Institute of Theoretical Geophysics, Department of Applied Mathematics and Theoretical Physics, University of Cambridge, Cambridge CB3 0WA, UK. (rs620@cam.ac.uk)

0094-8276/13/10.1002/2013GL057942

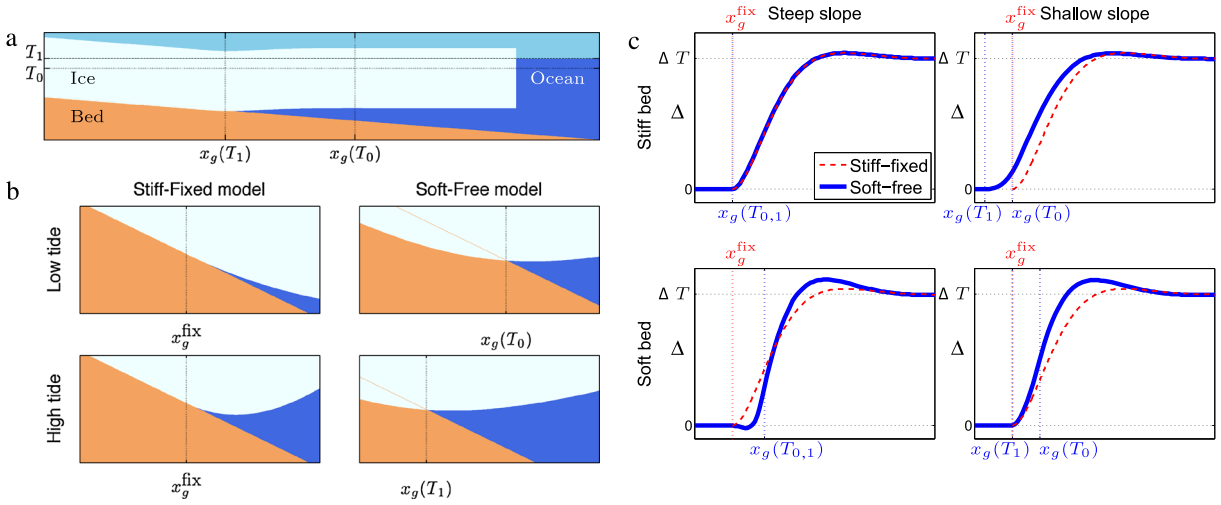

Figure 1. (a) A schematic showing the deflection of an ice sheet that is supported by a bed and an ocean. A change of sea level from T_0 to T_1 by tidal action forces the GL to migrate from $x_g(T_0)$ to $x_g(T_1)$. (b) Close-ups to the region near the GL. In a stiff-fixed model the ice curvature at the GL $x_g^{\rm fix}$ increases with the tide (on the bed profile considered here), whereas in the soft-free model, the curvature does not change while the GL adjusts. (c) Tidal curves in stiff-fixed models (- - - -) are zero upstream of the fixed GL unlike those of the soft-free model (——). Differences between stiff-fixed and soft-free models are small on steep slopes and stiff beds but increase on softer beds owing to differences in the curvature and on shallower slopes owing to larger GL migration.

constant of the underlying bedrock plus the water-till mixture, having stiffnesses k_b and k_t, respectively, whence $1/k_0 = 1/k_t + 1/k_b$. We can estimate each stiffness using Hooke's law as σ/δ, where σ is the normal pressure and δ is the vertical displacement of the bed. The displacement of a till having thickness h and Young's modulus E_t is $\delta = \sigma h/E_t$. The bedrock can be modeled as an elastic medium with Young's modulus E_b that occupies a half space, implying $\delta \simeq \sigma R/E_b$, where R is the horizontal range along which pressure is applied [*Landau and Lifshitz*, 1970]. The bed and the till stiffnesses are therefore $k_t = E_t/h$ and $k_b = E_b/R$, respectively. The till can be of order 1 m thick with E_t ranging between 1 MPa for soft till [*Walker et al.*, 2013] and 1.5 GPa for overconsolidated till [*Bell*, 2000], implying $k_t \approx 1$ MPa/m for thick, dilatant till or 10 GPa/m for thin, dense till. For the bedrock, $E_b \approx 500$ GPa [*Turcotte and Schubert*, 2002], while $R \approx 10^2 - 10^4$ m represents the range over which the GL migrates, implying that $k_b \approx 10 - 1000$ MPa/m. Therefore, k_0 ranges from about 1 MPa/m to about 1 GPa/m.

[7] Testing the consistency of elastic theories with observations requires the removal of long-time-scale footprints of viscous deformation in the observational data. This is achieved by considering the *tidal curve* Δy, defined as the difference between two deflection curves measured at tidal phases with amplitudes T_1 and T_0, and corresponding GL positions $x_g(T_1)$ and $x_g(T_0)$ (Figures 1a and 1c and supporting information).

3. Analysis and Implications

3.1. Consistency With the Young's Modulus of Ice

[8] We now consider the tidal curve measured across the grounding zone of Rutford Ice Stream, Antarctica (Figure 2), starting above a steep knoll in the center of this 30 km wide stream of nearly uniform thickness. Regression to a stiff-fixed model with tidal difference $\Delta T = T_1 - T_0$, GL position $x_g^{\rm fix}$ and Young's modulus E as free parameters implies $E \approx 1.8$ GPa – about 5 times less than the value found by laboratory measurements. In contrast, the regression to the soft-free model is performed with a constant Young's modulus of 9.33 GPa given by the laboratory measurements and with the same number of free parameters as in the stiff-fixed

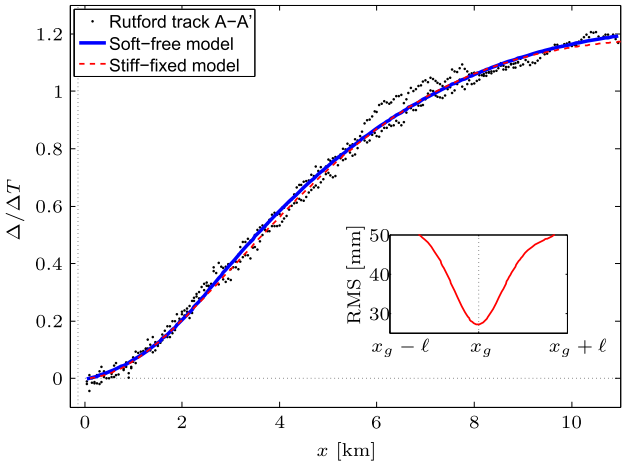

Figure 2. Tidal curve (solid circle) that was measured along a flow line of the Rutford Ice Stream, Antarctica [*Vaughan*, 1995] (supporting information). Regression to the stiff-fixed model predicts (- - - -) $\Delta T \approx 4.1$ m, $x_g^{\rm fix} = -60 \pm 0.9$ m and $E = 1.86$ GPa with $\sim$ 26 mm root-mean-square (RMS) error. Regression to the soft-free model with $E = 9.33$ GPa, $H = 1550$ m, and $S = 3/100$ [*Rignot*, 1998] (——) predicts $\Delta T \approx 4.08$ m, $x_g(T_1) \approx -135 \pm 0.9$ m, and $k_0 \approx 1.6$ MPa/m, with $\approx$ 27 mm RMS error (inset), implying that within a tidal cycle with amplitude of 4 m, this GL migrates about 270 m $\ll \ell$, as expected on steep slopes.

case, given by $\Delta T, x_g(T_1)$ and the bed stiffness k_0. The result (Figure 2) shows excellent agreement with the data, indicating $k_0 \approx 1$ MPa/m and a GL position nearly 75 m upstream from that set by the stiff-fixed model. This agreement is possible within the soft-free model, despite the substantially larger elastic modulus, owing to the capacity of the bed to deform and the consequent unconstrained ice slope at the GL. In addition, the fact that $\ell \propto E^{1/4}$ implies that a factor five increase of Young's modulus results in ℓ growing by only about 50%. Such consistency of the purely elastic, soft-free model both with the flexure data and with the known elastic properties of ice provides an alternative interpretation of the dominant underlying processes, suggesting that viscous interpretations may not always be relevant.

[9] The resultant bed stiffness, implying 1 m vertical displacement, and the small range of GL migration indicate the presence of a thick layer of subglacial material having the capacity to become highly dilatant, which may be consistent with some observations beneath Rutford Ice Stream [*King et al.*, 2009]. It is conceivable that ℓ is effectively smaller, owing to nonuniform ice density and surface fractures that imply smaller effective thickness or Young's modulus or larger Poisson ratio [*Jenkins et al.*, 2006], which would lead to a larger bed stiffness and smaller displacement. In addition, the knoll beneath the stream is a significant disruption to the bed slope, which requires a more detailed analysis. We note that similar bed stiffness values in a soft-bed and fixed-GL model [*Walker et al.*, 2013] imply smaller bed compression since the grounded ice is pinned at both ends.

3.2. Grounding Line Migration Between High and Low Tides

[10] The explicit coupling of the GL position and the tidal amplitude in the soft-free model becomes important when resolving GL migration on shallow slopes such as ice plains. We use altimetry measurements taken in tidal phases T_0, T_1 and T_2 at two locations in the Filchner-Ronne grounding zone and compute regressions to two tidal curves at each location (supporting information). Regression to the stiff-fixed model is computed separately for each of the curves (as in §3.1), since the GL and the tidal phase are not coupled. Using ΔT, x_g and Young's modulus as fitting parameters for each curve (six parameters in all), we find that a good agreement between this model and the data (Figure 3) is not obtained unless Young's modulus is dependent on phase [*Schmeltz et al.*, 2002]. Regressions to the soft-free model are computed to both tidal curves simultaneously using fewer (five) fitting parameters, namely $T_{0,1,2}$, k_0 and the GL position at T_0. The results provide better agreement between the theory and the data than the stiff-fixed model, despite the fewer fitting parameters. They indicate that $k_0 \approx 7.6$ GPa/m ($\delta \sim 1.3$ mm), consistent with GL migration of 4.1 ± 0.1 km at one track (Figure 3a) and $k_0 \approx 6.3$ GPa/m ($\delta = 1.4$ mm) with GL migration of 13.3 ± 0.2 km at another (Figure 3b). The dimensional analysis in §2 suggests that such GL migrations should correspond to softer beds (about 10–100 MPa/m). However, it is conceivable that the large ice rise a few tens of kilometers downstream of the GL along these tracks, a distance comparable to $\ell \approx 32$ km, pins the shelf even at high tide so that the tidal response at this location involves substantial tension, which the present theory does not account for.

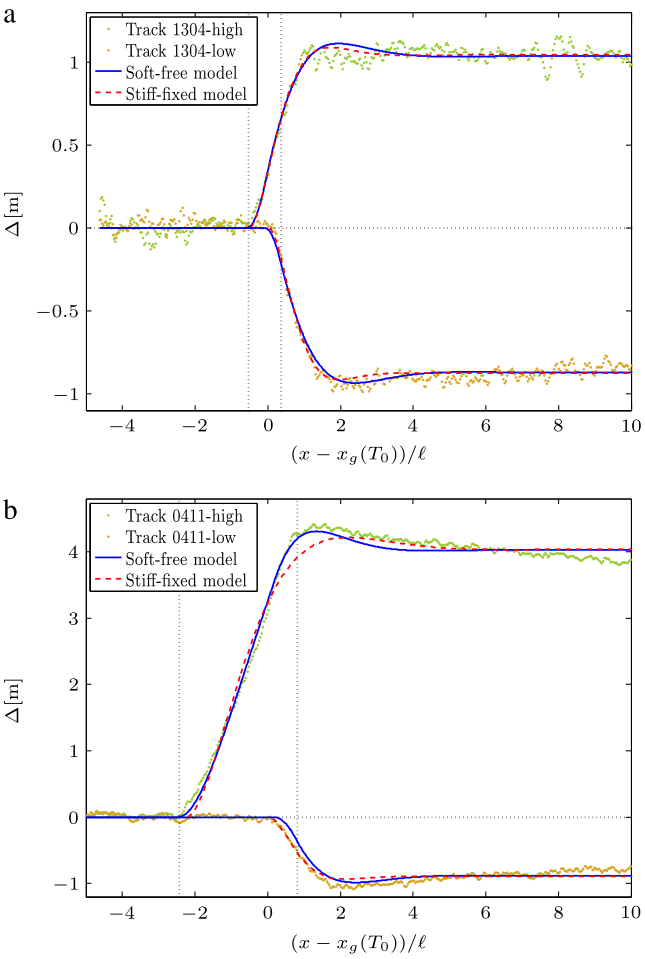

Figure 3. Tidal curves formed by satellite-based laser altimetry (•,•) along two tracks in Filchner-Ronne grounding zone [*Brunt et al.*, 2011; *Fricker and Padman*, 2006] (supporting information). Regression to the soft-free model (——) results in $k_0 \approx 7.6$ GPa/m and tidal amplitudes $T_{0,1,2} \approx 0.16, 1.2, -0.71$ m, with 50 mm RMS error for (a) track 1304, and in $k_0 \approx 6.3$ GPa/m and tidal amplitudes $T_{0,1,2} \approx -0.34, 3.69, -1.22$ m with 86 mm RMS error for (b) track 411. Regression to the stiff-fixed model (- - - -) results in similar tidal amplitudes, yet with phase-dependent Young's modulus equal to 2.35 GPa at high tide and 1.3 GPa at low tide for track 1304, and to 44 GPa at high tide and 2.2 GPa at low tide for track 411. Left/right grid lines mark the GL at high/low tide.

[11] As the GL migrates at high tide, the contact area between the ice base and the ocean increases. Although this increase can be small compared with the length of an ice shelf, the impact on basal melting can be substantial, because the maximum melt rate that is driven by the ocean thermal forcing occurs near the GL in a small region compared with the shelf length [*Jenkins and Doake*, 1991; *Rignot et al.*, 2013].

3.3. The Impact of Basal Deformation on Subglacial Hydraulics

[12] The deformation of the bed under the elastic pressure of the ice has significant implications for subglacial hydrology and lubrication near the GL. A subglacial hydraulic

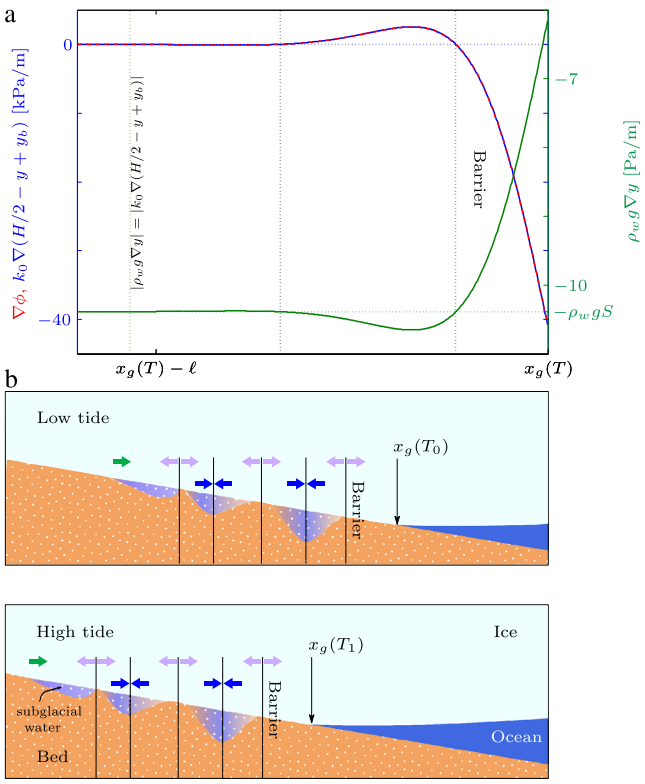

Figure 4. (a) The subglacial hydraulic potential $\nabla\phi$ (- - -) along the grounded ice (k_0 = 100 MPa/m, S = 1/1000). Near the GL, it is elastically controlled and oscillatory (——), while further upstream it is dominated by the hydrostatic water pressure (——). (b) Schematic cross sections of the grounding zone, showing the migration of the hydraulic barrier ($\nabla\phi$ = 0) and of the subglacial water system as the GL migrates between low and high tides, where arrows mark the flow direction of subglacial water. The positions where $\nabla\phi$ = 0 are marked by vertical, dark grid lines.

potential that accounts for the ice elastic pressure is $\phi = \rho_w g y + \rho_i g H + D\nabla^4 y$, which together with equation (1) implies a gradient of the subglacial hydraulic potential, $\nabla\phi = \rho_w g \nabla y + k_0 \nabla (H/2 - y + y_b)$. Far from the GL, the elastic pressure in the ice diminishes, leading to $y \approx y_b + H/2$ and therefore to $\nabla\phi \approx -\rho_w g S \approx \mathcal{O}(1 - 10$ Pa/m). However, bending of the ice near the GL enhances the elastic pressure substantially, leading to $\nabla\phi \approx -k_0 (S + \nabla y) \approx \mathcal{O}(10^3$ Pa/m) over a distance of the order of ℓ, in which the gradient of the hydraulic potential is negative close to the GL and positive further upstream (Figure 4a). Consequently, this elastically controlled region acts as a barrier that prevents leakage of subglacial melt water toward the ocean and transfer of ocean water landward.

[13] A large tidal migration of the GL on shallower slopes combined with the action of the elastically dominated hydraulic barrier can potentially control subglacial lubrication (Figure 4b). At high tide, the landward migration of the hydraulic barrier can also force the subglacial water system to migrate, increasing the area of subglacial lubrication that could consequently trigger a slip action [*Bindschadler et al.*, 2003; *Anandakrishnan et al.*, 2003]. At low tide, the hydraulic barrier migrates toward the ocean, thereby reducing the lubricated area while pushing ocean water downstream. The larger $\Delta T/S/\ell$ is, the larger the hydraulic barrier migration and the potential for extended slip conditions at high tide. Therefore, ice located on wet beds and shallow bed slopes (e.g., ice streams) is more likely to undergo slip events under this mechanism. This outcome is in contrast with the case of a pinned GL [*Walker et al.*, 2013], in which the elastic pressure gradient changes sign at low tide, implying suction of ocean water into the subglacial domain. These considerations indicate a mechanism by which subglacial water can be redistributed but much more detailed modeling of the subglacial hydrology is required to assess this potential.

4. Conclusions

[14] Our analysis coupling the grounded sheet to the floating shelf demonstrates that the grounding line can migrate several kilometers during a tidal cycle (estimated at 13 km at one location of Filchner-Ronne ice shelf, for example), implying that at high tide the area of ice that undergoes basal melting at maximum rate is larger. It also shows that at high tide subglacial lubrication is enhanced, which provides an explanation for the observed slip action associated with tides. Consequently, these processes can combine to accelerate the transfer of mass from ice sheets to the ocean, making it essential to account for such processes on tidal timescales in order to improve the prediction of the mass balance of ice sheets and ultimately of sea level rise.

[15] **Acknowledgments.** We thank D. Vaughan and J. Neufeld for commenting on this manuscript and J. Lister for discussions. We also thank D. Vaughan for providing the data in Figure 2 and to K. Brunt, M. Siegfried, and H. A. Fricker for providing the data in Figure 3.

[16] The Editor thanks two anonymous reviewers for assistance evaluating this paper.

References

Anandakrishnan, S., D. E. Voigt, R. B. Alley, and M. A. King (2003), Ice stream D flow speed is strongly modulated by the tide beneath the Ross Ice Shelf, *Geophys. Res. Lett.*, *30*(7), 1361, doi:10.1029/2002GL016329.

Anandakrishnan, S., G. A. Catania, R. B. Alley, and H. J. Horgan (2007), Discovery of till deposition at the grounding line of Whillans Ice Stream, *Science*, *315*(5820), 1835–1838.

Bell, F. (2000), *Engineering Properties of Soils and Rocks*, 482p. 4th edn, Blackwell Science, Oxford, U. K., Malden, Mass.

Bindschadler, R. A., M. A. King, R. B. Alley, S. Anandakrishnan, and L. Padman (2003), Tidally controlled stick-slip discharge of a West Antarctic ice, *Science*, *301*(5636), 1087–1089.

Brunt, K. M., H. A. Fricker, and L. Padman (2011), Analysis of ice plains of the Filchner-Ronne Ice Shelf, Antarctica, using ICESat laser altimetry, *J. Glaciol.*, *57*(205), 965–975.

Fricker, H. A., and L. Padman (2006), Ice shelf grounding zone structure from ICESat laser altimetry, *Geophys. Res. Lett.*, *33*, L15502, doi:10.1029/2006GL026907.

Gammon, P. H., H. Kiefte, M. J. Clouter, and W. W. Denner (1983), Elastic constants of artificial and natural ice samples by Brillouin spectroscopy, *J. Glaciol.*, *29*(103), 433–460.

Gudmundsson, G. H. (2006), Fortnightly variations in the flow velocity of Rutford Ice Stream, West Antarctica, *Nature*, *444*(7122), 1063–1064.

Gudmundsson, G. H. (2011), Ice-stream response to ocean tides and the form of the basal sliding law, *Cryosphere*, *5*(1), 259–270.

Holdsworth, G. (1977), Tidal interaction with ice shelves, *Ann. Geophys.*, *33*(1-2), 133–146.

Jacobel, R. W., A. Robinson, and R. A. Bindschadler (1994), Studies of the grounding-line location on Ice Streams D and E, Antarctica, *Ann. Glaciol.*, *20*(1), 39–42.

Jenkins, A., and C. S. M. Doake (1991), Ice-ocean interaction on Ronne Ice Shelf, Antarctica, *J. Geophys. Res.*, *96*(C1), 791–813.

Jenkins, A., H. F. J. Corr, K. W. Nicholls, C. L. Stewart, and C. S. M. Doake (2006), Interactions between ice and ocean observed with phase-sensitive

radar near an Antarctic ice-shelf grounding line, *J. Glaciol.*, *52*(178), 325–346.

King, E. C., R. C. A. Hindmarsh, and C. R. Stokes (2009), Formation of mega-scale glacial lineations observed beneath a West Antarctic ice stream, *Nat. Geosci.*, *2*(8), 585–588.

Landau, L., and E. Lifshitz (1970), *Theory of Elasticity*, 165p. 2nd ed., vol. 7, Pergamon, Oxford, U. K.

Reeh, N., E. Christensen, C. Mayer, and O. Olesen (2003), Tidal bending of glaciers: A linear viscoelastic approach, *Ann. Glaciol.*, *37*, 83–89.

Rignot, E. (1996), Tidal motion, ice velocity and melt rate of Petermann Gletscher, Greenland, measured from radar interferometry, *J. Glaciol.*, *42*(142), 476–485.

Rignot, E. (1998), Radar interferometry detection of hinge-line migration on Rutford Ice Stream and Carlson Inlet, Antarctica, *Ann. Glaciol.*, *27*, 25–32.

Rignot, E., J. Mouginot, and B. Scheuchl (2011), Antarctic grounding line mapping from differential satellite radar interferometry, *Geophys. Res. Lett.*, *38*, L10504, doi:10.1029/2011GL047109.

Rignot, E., S. Jacobs, J. Mouginot, and B. Scheuchl (2013), Ice-shelf melting around Antarctica, *Science*, *341*(6143), 266–270.

Sayag, R., and M. G. Worster (2011), Elastic response of a grounded ice sheet coupled to a floating ice shelf, *Phys. Rev. E*, *84*, 036111.

Schmeltz, M., E. Rignot, and D. Macayeal (2002), Tidal flexure along ice-sheet margins: Comparison of InSAR with an elastic-plate model, *Ann. Glaciol.*, *34*, 202–208.

Sykes, H. J., T. Murray, and A. Luckman (2009), The location of the grounding zone of Evans Ice Stream, Antarctica, investigated using SAR interferometry and modelling, *Ann. Glaciol.*, *50*(52), 35–40.

Turcotte, D. L., and G. Schubert (2002), *Geodynamics*, 456p. 2nd ed., Cambridge Univ. Press, Cambridge.

Vaughan, D. G. (1995), Tidal flexure at ice shelf margins, *J. Geophys. Res.*, *100*(B4), 6213–6224.

Walker, R. T., B. R. Parizek, R. B. Alley, S. Anandakrishnan, K. L. Riverman, and K. Christianson (2013), Ice-shelf tidal flexure and subglacial pressure variations, *Earth Planet. Sci. Lett.*, *361*, 422–428.